Journal of Manufacturing Processes 69 (2021) 583–592

Contents lists available at ScienceDirect

Journal of Manufacturing Processes

journal homepage: www.elsevier.com/locate/manpro

Humidity-controlled direct ink writing for micro-additive manufacturing with water-based inks

Kevin T. Estelle, B. Arda Gozen *

Washington State University, School of Mechanical and Materials Engineering, United States of America

ARTICLE INFO

Keywords:
3D bioprinting
Bioinks
Hydrogels
Extrusion-based additive manufacturing
Water-soluble polymers

ABSTRACT

Direct-ink-writing type additive manufacturing with water-based inks such as hydrogels or polymer solutions is broadly utilized for bioprinting applications. However, the resolution of this implementation is limited due to the rapid ink drying experienced at small size scales leading to nozzle clogging and low fidelity prints. To address this issue, a humidity-controlled direct-ink-writing (HCDIW) approach is presented, where the microenvironment around the printing nozzle is controlled through introduction of aerosolized water. Using this approach, the nozzle microenvironment can be varied between undersaturated yet high relative humidity (ambient to 100% RH) to oversaturated conditions where condensing droplets are deposited on the already printed ink filaments. The influence of the aerosolized water and the resultant micro-environment on the printing process was studied using water dissolved sodium carboxymethyl cellulose (NaCMC) ink, specifically focusing on nozzle clogging, printed filament geometry, surface quality and layer by layer stacking. These studies showed that the ink drying induced nozzle clogging issues can be mitigated through increased relative humidity at the nozzle exit and is virtually eliminated for ~100 μm nozzles in oversaturated conditions. The decelerated ink drying under the effect of aerosolized water leads to reduced solute advection and skin formation. This in turn improves surface roughness while reducing adverse effects such as coffee-ring and void formation during additive manufacturing of micro-scale structures. Furthermore, layer-to-layer fusion and associated side-surface quality were improved specifically in undersaturated conditions. Reduction of deposited ink filament concentration in oversaturated conditions leads to excessive spreading of the deposited inks leading to geometric distortions. These results indicate that the humidity control approach can significantly improve the resolution of the direct-ink-writing approaches, enabling processing of water-based inks at micro-scales.

1. Introduction

The recent emergence of personalized medicine has led to a demand for customizable biomedical devices and living products such as artificial organs [1]. Realization of the full potential of such technologies relies on their capability to work with the human body, necessitating conformance to and/or mimicry of its features. These requirements manifest in highly complex, heterogeneous designs consisting of several materials posing a significant manufacturing challenge. Inherent capabilities of additive manufacturing offer a great potential to address this challenge, which led to the emergence of the bioprinting technologies involving additive processing of bio-relevant materials, strengthened by other emergent design and process control approaches [2–4]. As such, there is a pervasive need for research to understanding the fundamentals and improving the key capabilities of bioprinting towards successful advancement of personalized medicine.

One of the most commonly used approaches for bioprinting is direct-ink-writing (DIW) [2] which involves controlled flow of materials through nozzles and their deposition on to substrates layer-by-layer. DIW can process a broad range of materials including biomaterial-laden hydrogels and water-soluble polymers (referred to generally as "bioinks") that are difficult to process by other additive manufacturing methods due to their complex rheological properties and need for maintaining the viability of the biomaterials they carry. Furthermore, the DIW can easily deposit multiple materials in a single part towards achieving biomimicking heterogeneity. One critical limitation of the DIW method preventing its broader industrial adaptation in biomedical applications is its resolution which is generally limited to hundreds of microns [5] which is an order of magnitude larger than the feature detail of many biological systems [6,7]. For most bioinks, the primary reason

* Corresponding author.
E-mail address: arda.gozen@wsu.edu (B. Arda Gozen).

https://doi.org/10.1016/j.jmapro.2021.07.059
Received 4 April 2021; Received in revised form 19 July 2021; Accepted 29 July 2021
Available online 18 August 2021

behind this limitation is the rapid ink drying at small scales, due to the high surface area to volume ratio of the extruded filaments [8]. Because the ink solvent evaporates so quickly at these size scales, leaving a clump of solute at the nozzle end, ink drying causes frequent nozzle clogging particularly for nozzles smaller than 100 μm. This directly limits the printing resolution and consequently the achievable print feature definition. Additionally, rapid drying of the surfaces of the previously deposited layer prevents formation of robust layer-to-layer fusion, leading to poor mechanical properties and high surface roughness [9]. A variation of the DIW method involving printing inside a support gel [10] or electrolytic solutions [11] can mitigate the drying issue while generating high resolution features [12,13]. However, these processes are only compatible with bioinks that have specific cross-linking mechanisms [11,14]. They also necessitate support media to be evacuated completely from the printed structures which is specifically challenging with small scale parts [15]. Finally, these approaches work well for bioprinting applications where complete prevention of the ink drying is favorable, such as hydrogel tissue scaffolds that hold up over 90% water by volume [16]. However, there are several applications involving the use of non-crosslinked water-soluble polymers where the final product is dry and rigid such as dissolvable micro needle arrays [17] or functional thin films [18]. As such there is a need for a comprehensive understanding of the drying process during DIW and how it influences the process outcome at small scales as well as practical methods to regulate such effects for a broad range of bioinks.

One way to regulate ink drying is to control the humidity level of the environment around the printing nozzle and deposited structure [19,20]. In this paper, a humidity controlled DIW configuration (HCDIW) is presented to achieve this control. HCDIW employs two concentric nozzles, where the inner nozzle carries and extrudes the water-based ink and the outer nozzle supplies a stream of air containing aerosolized water droplets from a nebulizer to the printing zone to control the local humidity condition as illustrated in Fig. 1. The aerosolized water effectively generates a low concentration zone right outside the nozzle and its vicinity on the recently printed parts of the print (Fig. 1(b)) by slowing down the drying process, or, by depositing excess amounts of aerosolized water, actively increasing the water content. Through the regulation of the ink drying, HCDIW aims to mitigate nozzle clogging, improve the fusion of the deposited filaments and layers and accordingly improve the quality of the printed parts. In the following sections, details of this system's configuration and methods to precisely regulate the environment around the printing process are introduced. The results from the printing studies with water soluble sodium carboxymethyl cellulose inks to fabricate dry, micro-scale structures are then presented. Particularly, the effects of the supplied aerosolized air amount (and the associated local humidity at the nozzle exit) on nozzle clogging, printed filament geometry, layer-to-layer fusion, and side wall morphology of the printed structures are studied.

2. Methods and materials

2.1. Materials

In this study, an aqueous sodium carboxymethyl cellulose (NaCMC) solution was used as a bioink at a fixed concentration of 20% w/w. To prepare the inks, first a dilute solution was prepared by mixing 3 g of NaCMC (90 kDa, Sigma Aldrich) with 30 ml deionized water using a high-speed mixer (Cole-Parmer Compact Digital Mixer System) overnight at 350RPM. The ink is then reweighed to account for losses during stirring and placed in a vacuum-oven (Lindberg Blue M Thermo-Scientific) at 60 °C and 25 inHg vacuum to evaporate the excess water for 4 h. The ink is then stored in a closed glass jar at 8 °C to mitigate mold growth and solvent evaporation. Just before printing, the ink is transferred into a 3 cc syringe, brought back up to ambient temperature, and centrifuged (Nordson EFD ProcessMate™ 5000, PLC-012) for 10 min at 6000RPM to remove air bubbles. The produced inks exhibit Herschel-Bulkley [21] type rheological behavior with yield stress and shear thinning properties as shown in the supporting information, Section S1.1.

2.2. DIW system

3D printing was performed using a custom direct ink writing setup as shown in Fig. 2. This system includes a 3-axis motion system (Aerotech ANT180-ANT130 stages), which hosts the build plate and translates it in three dimensions with sub-micron accuracy. A micro-dispensing positive-pressure pump system (nScrypt SmartPump) serves as the printhead and regulates the ink flow from a reservoir to a print nozzle through the vertical position of a needle valve. Surrounding the entire head and print nozzle is a custom-made outer humidity nozzle held in place by the 3 cc syringe that is set into the side syringe port. Nozzles with 120 μm inner diameter (Nordson 7018462) have been used. This system also features

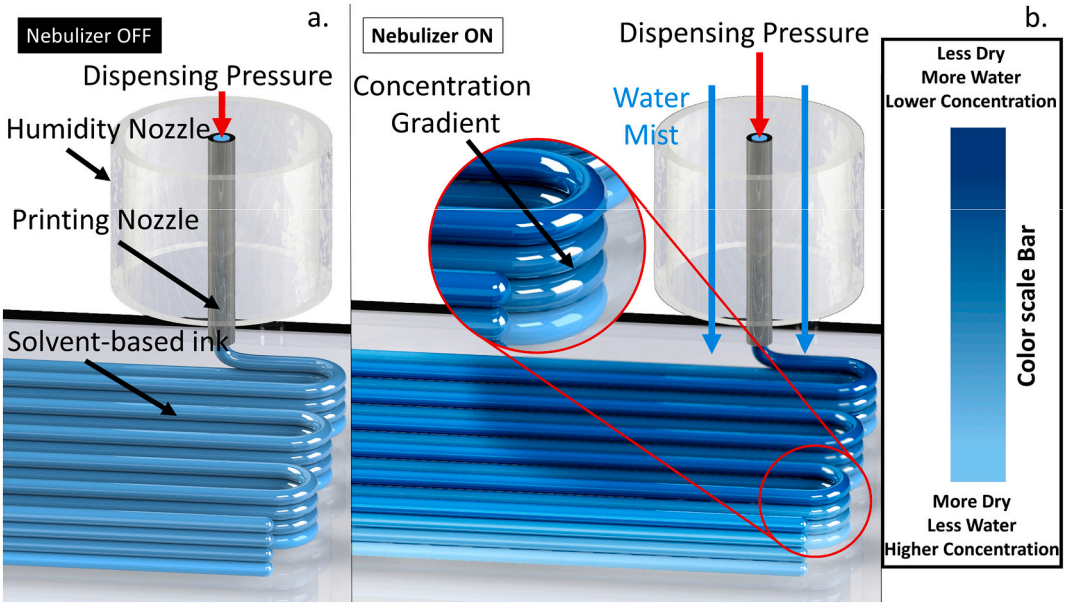

Fig. 1. Schematic description of HCDIW and the induced concentration gradient in the printed part.

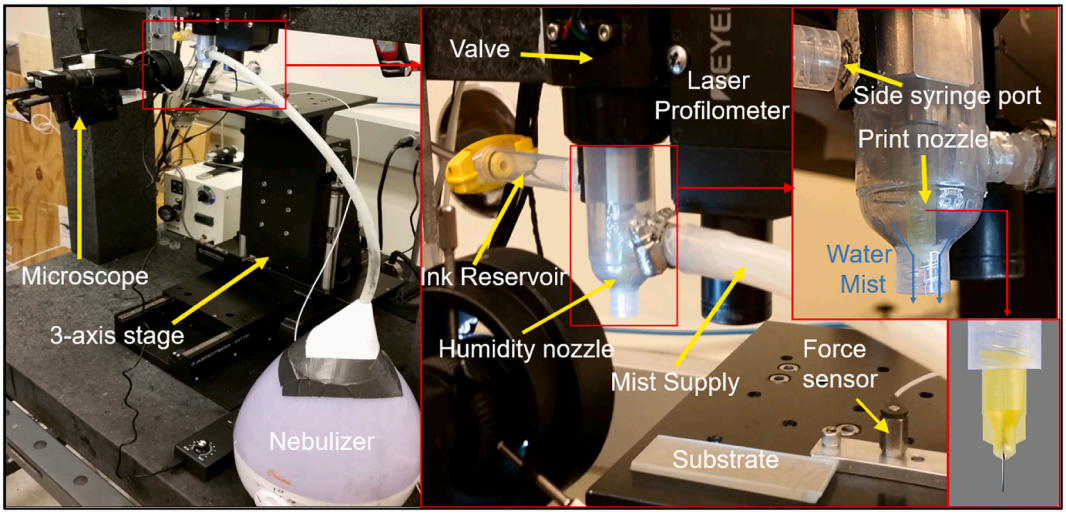

Fig. 2. Printing setup.

two metrology tools: a piezoelectric force sensor (PCB Piezotronics 484B06) and a laser displacement sensor (Keyence LT9031M), both of which are used to measure the distance between the nozzle and the substrate and precisely control nozzle-standoff distance (see section S1.2 in the supporting information). The entire system is controlled through a LabView interface that is capable of executing automated printing and metrology tasks by controlling the motion stages, the print head, the force sensor, and the laser displacement sensor. To visually monitor the printing process, a microscope camera (Sentech STC MCCM200U3V) was integrated into the system. All prints were done on glass slide substrates.

2.3. Humidity control setup

The setup used to control the aerosolized water flow through the humidity nozzle is shown in Fig. 3(a). Aerosolized water droplets are formed inside the nebulizer (Crane Drop Shape Ultrasonic Cool Mist Humidifier, [1 gal capacity, max flow rate 0.02 ml/min]), are passed up through the servo-controlled valve, and into the humidity nozzle to be delivered to the printing zone. The humidity condition at the end of the printing nozzle using this system is controlled through two inputs, one is the nebulizer level and the other one is a servo-valve position θ as shown in Fig. 3(a). To control the humidity level at the end of the printing nozzle between 0 and 100% relative humidity (RH), referred to as under-saturated conditions, the nebulizer level is set to 1/100th to 1/

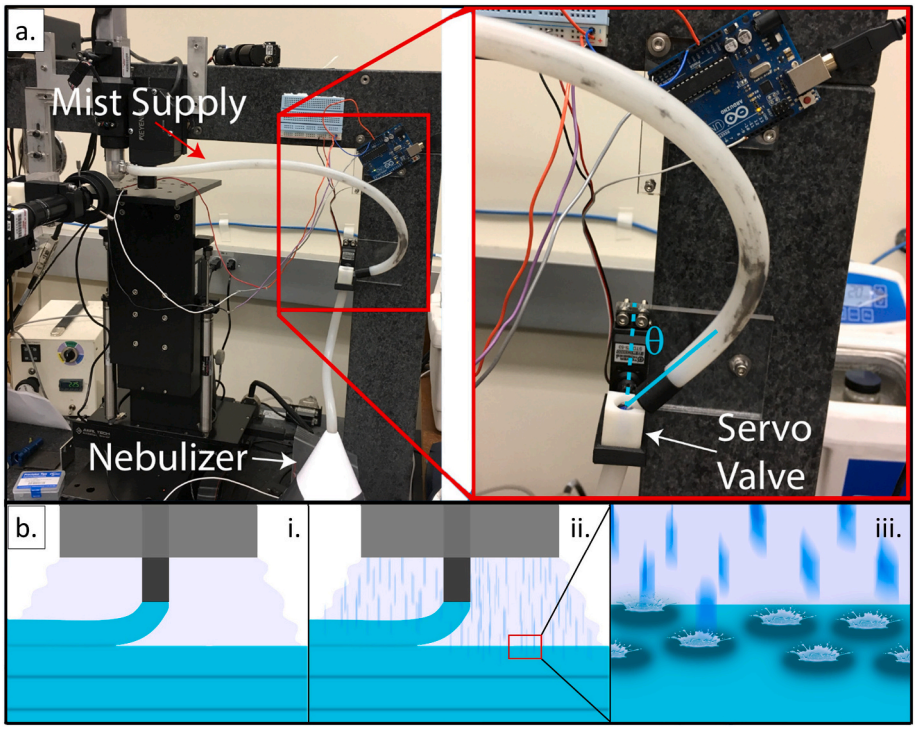

Fig. 3. Humidity control system and various modes of operation (a) Components of the humidity control setup. (b)(i.) Undersaturated printing 3(b)(ii.) Over-saturated printing 1.4(b)(iii.) Anticipated micro-concentration gradient on the printed structures during oversaturated printing. Darker colors in (iii.) denotes lower ink concentration (higher water content).

32nd of the full power (depending on the ambient humidity) and control the servo-valve position using an Arduino-based controller and a humidity sensor (HIH-4010-003 Honeywell sensing) to achieve a desired humidity level. The performance of this system for various target RH levels is demonstrated in Fig. S3 where the measured humidity level as a function of time is shown. To generate an over-saturated environment around the printing nozzle end, the servo-valve is bypassed completely, feeding the humidity nozzle with a hose directly from the nebulizer, and adjust the nebulizer level between 1/100th to 1/8th of the full power setting. In the oversaturated state, the water in excess of what ambient air can carry is deposited on the printed filaments to locally vary the ink concentration as shown in Fig. 3(b). After the desired humidity level is reached, the nozzle is moved to the starting printing position and an experiment started. For under-saturated conditions, the RH is re-checked and valve is readjusted periodically during the printing experiments by moving the nozzles back to the humidity sensor. Through this "pseudo" closed-loop approach, the variations on the RH level induced due to variations in the ambient humidity and temperature can be compensated.

2.4. Nozzle clogging tests

To study the influence of the humidity condition on nozzle clogging, tests were performed where ink flow under a dispensing pressure of 40 psi were periodically turned on and off. Initially, the flow valve was opened for 10 s and then closed for 30 s and reopened for 10 s to see if the nozzle tip clogged from ink drying during the off time. If the nozzle was not clogged, the valve was closed again, cleaned with a wet swab, and the wait time was increased by 30 s. Cleaning between each time and humidity condition increase was necessary to remove excess material at the nozzle tip and effectively reset the experiment.

2.5. Printing experiments

Two types of printing experiments were performed: (1) 10 mm long, 10-layer lines to study the influence of humidity control on the filamentary geometry and surface quality and (2) 1 mm × 1 mm × 0.5 mm pillars to study the influence of the humidity control on printed structure porosity and layer-to-layer fusion. For line prints, the humidity condition and printing speed were varied. The speed levels tested were 1, 2, and 3 mm/s for speed tests and 3 mm/s for all other lines prints, all at a printing pressure of 45 psi. Speed tests were conducted all on the same day and all parameters besides speed were held constant. The relative humidity levels were varied between ambient humidity to 100% in 20% increments, and four additional oversaturated conditions were tested by adjusting the nebulizer at 1/100th, 1/32nd, 1/16th, and 1/8th of the full power setting, represented in the rest of the paper by 1/100FS, 1/32FS, 1/16FS and 1/8FS, respectively.

Between each layer, the printhead was retracted 50 mm and the printing was paused for a certain dwell time to allow the previous layer to dry. For line prints, this dwell time was 60 s. Ten repetitions for each parameter set were performed by printing continuously in a serpentine pattern. For the pillars, the printing speed and pressure was kept constant at 1 mm/s and 40 psi respectively, and the humidity condition was varied. The structures were printed with rectilinear fill pattern at 100% infill and were 90 layers high. The layer height following the ink deposition and drying under a given condition were measured once using the laser interferometer and this measurement informed the vertical displacement of the substrate throughout the print. The layer height for pillars were 7 μm, while the dwell time between layers was 15 s for ambient and undersaturated conditions, 25 s for 1/100FS prints, 30s for 1/32FS prints, and 35 s for 1/16FS and 1/8FS prints. A detailed list of the experimental parameters used in these experiments is given in Table S1 and S2 in the supporting information Section 1.3.

2.6. Characterization of the printed structure geometry and morphology

A scanning electron microscope [SEM FEI Quanta 200F, ThermoFisher] was used to obtain secondary electron images the printed structures for qualitative inspection. An optical profilometer (Zygo NewView 6300) was used to quantitatively characterize the geometry of the prints and the raw data was analyzed using the freeware Gwyddion software. Fig. 4 shows the details of the profilometry analysis for the 10-layer line prints. As shown in the inset of Fig. 4(a), the first layer exhibited higher width than the subsequent layers, since the surface energy between the ink and the substrate is higher than the ink and the previously deposited layers. As such, the first layer of the prints was excluded from the analysis to get a more objective measure of the 3D line geometry. To this end, single layer prints were conducted for each experimental condition and measured to determine the part of the data to be excluded from the 10-layer. The rest of the data was used to determine the corrected height (H^*), width (w^*) and the cross-sectional area (A_{10}^*) of the lines as shown in Fig. 4(a). See Supporting Info Section S1.4 for the details of the calculations of these parameters. The RMS roughness of the top surface of the prints was determined also using the profilometry data within the region shown in Fig. 4(a).

For the pillars, the sidewall morphology was quantitatively analyzed by profilometry. To this end, the profilometry image of the pillar sidewalls was processed by subtracting an 11th order polynomial surface to remove the surface waviness and expose the periodic layered morphology as shown in Fig. 4(b). Next, average peak-to-valley height (PVH) in this morphology was calculated for different printing conditions. In that, the PVH from 20 layers were averaged per pillar. The PVH for a given peak was calculated as the mean of the distance between the peak and the two neighboring valleys as shown in Fig. 4(b), such that

$$PVH = (h_1 + h_2)/2 \quad (1)$$

The line prints imaged using SEM and all pillar prints were coated with gold using physical vapor deposition (Technics Hummer V Sputter Coater) to enhance their surfaces' the conductivity of for SEM images and reflectivity for profilometry.

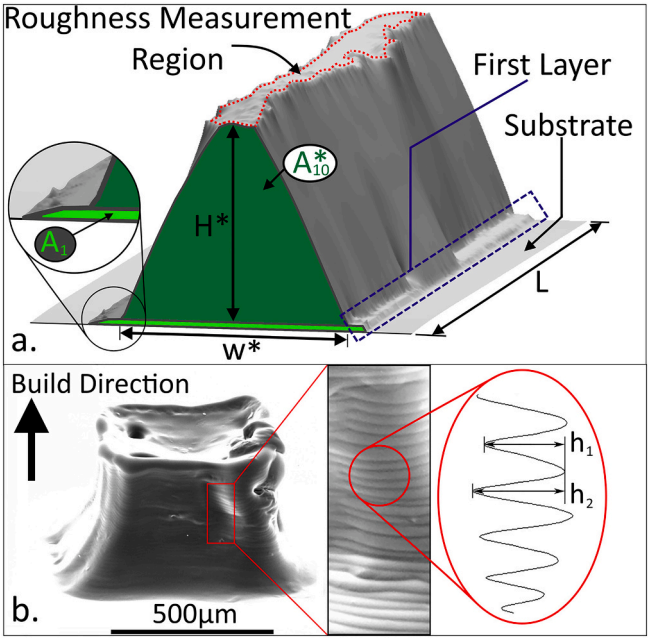

Fig. 4. Details of the geometric analysis (a) 10-layer line analysis, (b) pillar sidewall analysis.

3. Results and discussions

3.1. Mitigation of drying related printing issues

Fig. 5 details the amount of wait time (*i.e.* no flow) after which nozzle was clogged under different conditions. As shown, the length of this period increases with the amount of aerosolized water provided to the nozzle exit. In fact, for the over saturated conditions, no clogging was observed even after a wait time of 900 s, beyond which experimentation was not continued. Sample video recordings from these experiments are provided as supporting information. This result clearly indicates that the controlled humidity at the nozzle tip can be used as a tool to mitigate ink drying induced clogging for small nozzles and is likely due to the drying process being slowed by a concentration decrease in the ink as water is added to it. It should be noted that these tests were conducted when the ambient relative humidity was 38% RH. It is expected that the actual clogging time will vary with varying ambient humidity levels.

In addition to the mitigation of clogging, the general robustness and repeatability of the printing process was improved for the line and pillar printing experiments under increased humidity conditions. This was evident through many repeated experiments in which it was observed that when printing under ambient conditions, as shown in Fig. S4, a bridge of ink would form and dry between the printing nozzle and the already printed structure. Upon the retraction of the nozzle in preparation for a new print, this bridge would tear the current print of the substrate and/or slightly move the glass slides that were used as the substrates. Even if the print was not dislodged from the substrate, the movement of slides causes the next layer of the print to occur in the wrong position. Printing under humid conditions consistently prevented this ink bridge from drying likely due to the added water content to the ink bridge.

3.2. DIW line print experiments

Sample SEM images of 10-layer lines printed at a speed of 3 mm/s and a pressure of 45 psi are shown in Fig. 6 a, b, and c. Fig. 6 d, e, and f presents the dimensional analysis of the lines, outlining the variation of width, height, and cross-sectional area with the humidity condition. It can be seen in Fig. 6(d) that at a constant printing speed and pressure, cross-sectional area and therefore volumetric flow rate decrease as the amount of aerosolized water delivered at the nozzle exit is higher at ambient conditions. This finding indicates that ink viscosity is increasing with increasing amount of aerosolized water. Even though further analysis is required, one possible explanation for this is the cooling of the nozzles under the aerosolized water flow due to condensation of water droplets on the nozzle surface which in turn increases the viscosity of the ink flowing within. It should be noted that due to this variation in volume flow rate, error bars are relatively large in all result plots since the data presented is averaged across multiple days of printing where day-to-day ambient conditions changed beyond control. For this reason, a statistical analysis employing a two-sample equivalent variance *t*-test with a significance threshold value of 0.05 is applied to each result to confirm observed trends are viable and above the noise level of the data.

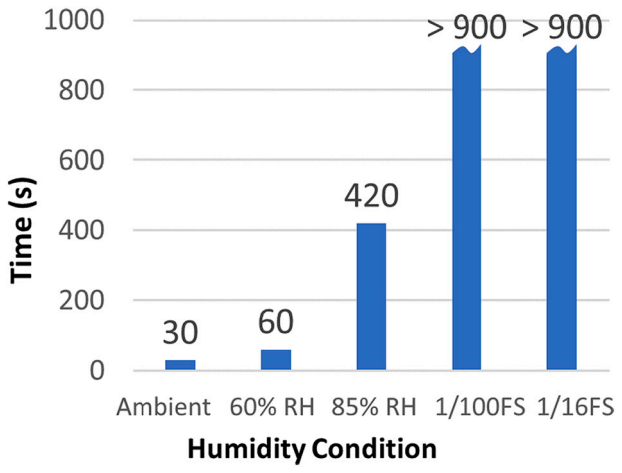

Fig. 5. Waiting (no-flow) time following which the nozzles were clogged under different humidity conditions.

3.2.1. Analysis of line geometry

The effect of the humidity condition on spreading of printed ink layers following deposition as a measure of multi-layer stacking performance was quantitatively evaluated firstly. High amounts of ink spreading is not ideal for multi-layer stacking as it increases the line-width, thus deteriorating in-plane resolution, while reducing layer height thus increasing the amount layers required to achieve a desired out-of-plane height of the printed structure. Due to the uncontrolled variation of the flow rate between the experiments as described above, to objectively compare the ink spreading under varying humidity conditions, a non-dimensional analysis approach was adopted. To quantify the degree of spreading, a non-dimensional spreading parameter derived through the geometric parameters outlined in Section 2.6 was used, given by

$$Spreading = \frac{w^{*2}k}{A^{*}_{10}} \tag{2}$$

where k is the layer count. Details of the derivation of this parameter are explained in depth in Supporting Information, Section S1.5. Fig. 7(a) summarizes the results of the spreading analysis for 10-layer prints, under varying humidity conditions at a printing speed of 3 mm/s. Here, a statistical analysis employing a two-sample equivalent variance *t*-test with a significance threshold value of 0.05 has been utilized to compare different humidity conditions. As shown, a significant increase in spreading has been observed for saturated conditions while spreading has been observed to be mostly non-variant between ambient and 80% RH humidity levels. Increased spreading at oversaturated conditions can be explained by the fact that ink concentration is decreased due to the amount of aerosolized water droplets absorbed by the printed ink as illustrated in Fig. 3(b). The reduced concentration in turn reduces the ink viscosity and increases the total drying time, both factors allowing the inks to flow and spread following deposition.

To build on the above result, how the exposure duration of the printed lines to the aerosolized water influences the spreading behavior was explored. To this end, the line spreading was characterized under oversaturated conditions and varying printing speeds, since with increasing speed, the printed lines are exposed to aerosolized water for a shorter duration, as the humidity nozzle travels over them. Here, 10-layer lines were printed at speeds of 1 mm/s, 2 mm/s and 3 mm/s at constant dispensing pressure. Fig. 7(b) shows the spreading values for ambient and three oversaturated conditions as normalized with respect to the average spreading value obtained at 1 mm/s, per humidity condition. As shown, no increased spreading was observed with decreasing speed (and thus increasing exposure duration) under oversaturated conditions, which is mostly consistent with the ambient conditions. In fact, a small statistically significant increase in spreading with increasing speed was observed at ambient and lowest tested humidity conditions. Further analysis with a larger set of data is required to conclude if this is an experimental aberration or an actual effect. These results indicate that the variation of exposure duration within the 1–3 mm/s range is not high enough to induce significant effects on line spreading. A better understanding of the timescale for decreased concentration induced spreading behavior can be obtained through Fig. S7, which shows an array of lines, only a portion of which were inadvertently exposed to aerosolized water (at 1/16 FS and 1/100FS) for multiple minutes after printing. The increased spreading of exposed portion

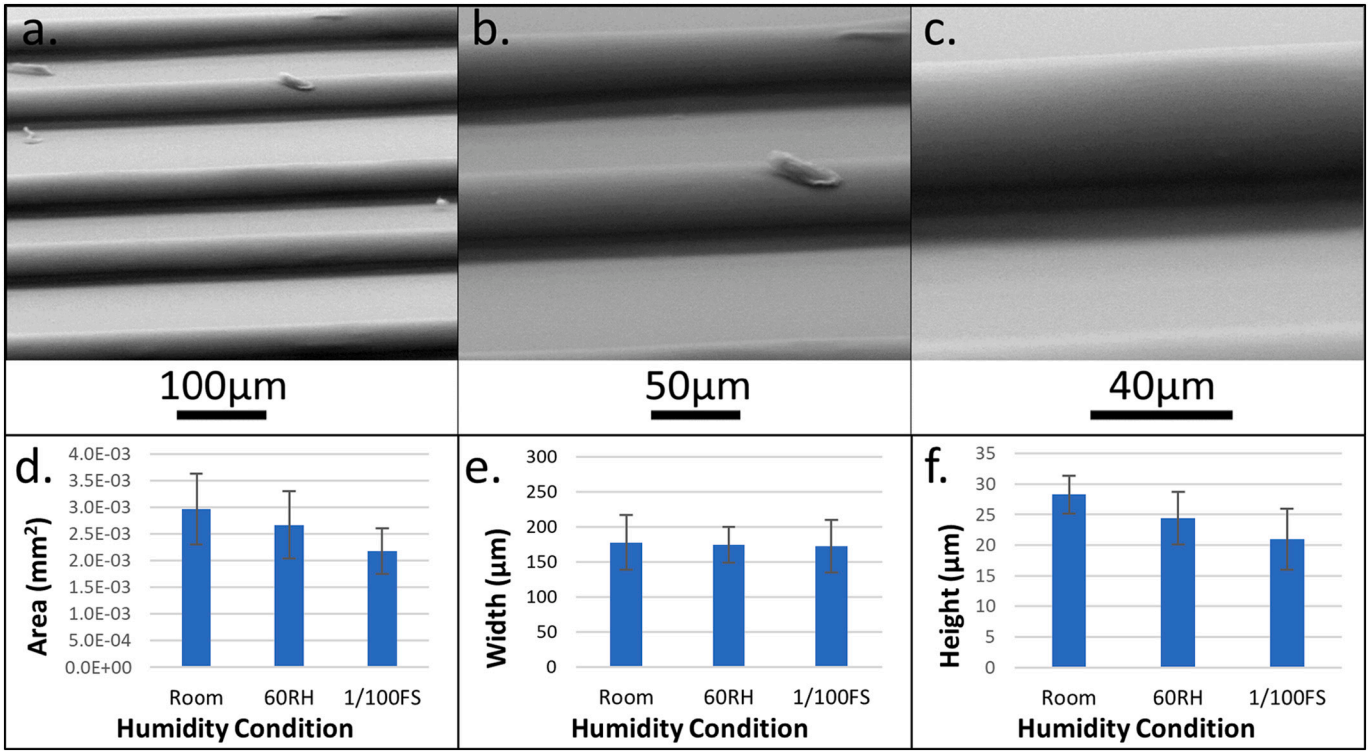

Fig. 6. SEM of Sample Line Prints (a, b, c) and Geometric parameters for the line prints: (d) Average cross-sectional areas, (e) widths, and (f) heights of 10-layer lines printed at 3 mm/s.

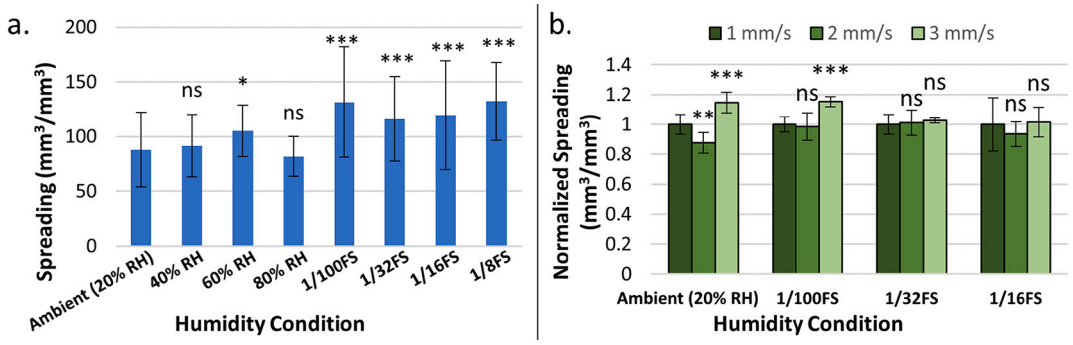

Fig. 7. Results of the spreading analysis (a) Spreading of 10-layer lines as a function of the humidity condition. Significance values were calculated with respect to the ambient condition data, (b) Spreading of lines at three printing speed as the humidity condition was varied between ambient to oversaturation levels. All significance values were calculated with respect to 1 mm/s data of each respective humidity condition.

confirms the influence of decreased concentration on spreading, particularly over the course of long exposure times.

In addition to the spreading of the lines, a coffee ring effect and its variation with the humidity condition as shown in Fig. 8 was also observed. This effect leads to formation of two distinct peaks at the top of the printed lines as highlighted in the cross-sectional profile of the 10-layer lines printed at 1 mm/s in Fig. 8(c). Here, H_{max} is the maximum z-coordinate observed among the two peaks, and H_{min} is the z-coordinate of the bottom trench. To quantitatively evaluate the effect of the humidity condition on the coffee ring formation, a non-dimensional analysis using a height-normalized difference between H_{max} and H_{min} was employed. Normalized trench height (H_n) is then given by

$$H_n = \frac{H_{max} - H_{min}}{H_{max}} \tag{3}$$

Results of the trench height analysis are shown in Fig. 8(d), considering the average of ten 10-layer lines per humidity condition. Consistent with the findings in the literature [20], the severity of the coffee ring effect is reduced with increased humidity condition due to reduced drying rate which increases the time-scale for drying process, reducing the solid convection speeds inside the inks leading to a more uniform solute distribution. It should be noted that the coffee ring effect was generally not observed for printing speeds higher than 1 mm/s. Given that the amount of material deposited per unit length decreases with increasing printing speed under constant flow rate, the total time required for a deposited line to dry will accordingly decrease. With that, it could be concluded that there is not enough time for the Marangoni flows to in evolve and create the coffee ring effects for those lines printed at high printing speeds.

3.2.2. Analysis of surface roughness

Fig. 9(a) shows RMS surface roughness of the lines printed at a speed of 3 mm/s as a function of humidity condition. As shown, the roughness generally reduced with increasing relative humidity through

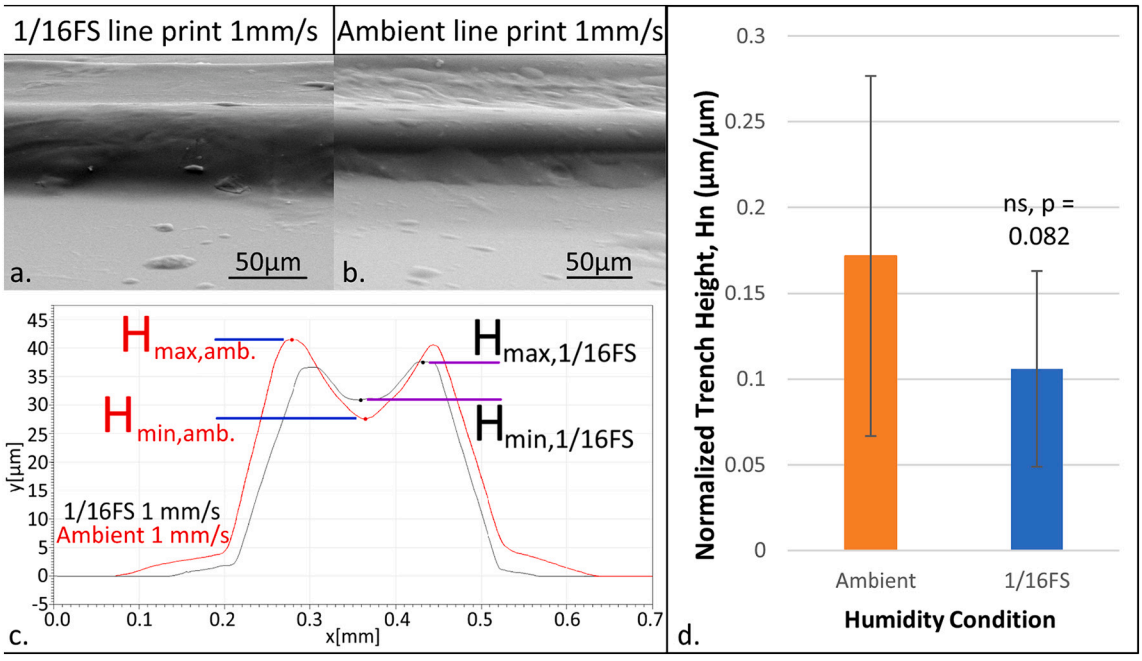

Fig. 8. Trench height analysis: SEM images of lines printed at (a) 1/16FS and (b) ambient conditions, both printed at 1 mm/s; (c) Average cross sectional profile comparing trench shape between the ambient to 1/16FS conditions, (d) Average normalized trench heights for each condition.

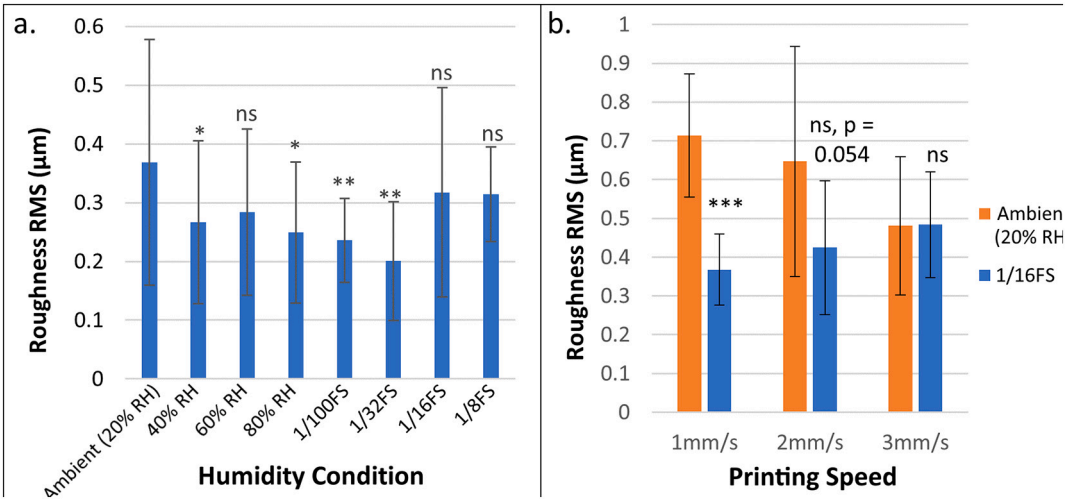

Fig. 9. Surface roughness analysis: (a) Roughness of 10-layer lines printed at 3 mm/s. (b) Roughness of 10-layer lines printed at 1 mm/s compared to ones printed at 3 mm/s printed at ambient and 1/16FS humidity conditions. All significance values are calculated with respect to 1 mm/s data of each respective humidity condition.

oversaturated conditions of 1/100 and 1/32 FS, while it increased with increasing aerosolized water flow over 1/32 FS level. The behavior between the ambient condition and the 1/32 FS level can be explained by reduction of the ink drying rate right after deposition due to the high humidity conditions. It has been shown by Strawhecker et al. [22] that roughness of the drying polymer solutions increases with increasing drying rate through several mechanisms. Primarily, at high evaporation rates, the time scale for the solvent evaporation is shorter than that for the solute to "flatten" during the drying process. For thicker films, high evaporation rates may lead to formation of a dry skin on the film-air interface, which in turn leads to solvent trapped underneath "bursting" out of the skin and generating nano-to-micro scale pinholes. Finally, high evaporation rates may lead to Marangoni instabilities for low viscosity solutions. Considering the relatively high concentration (20% *w*/w) of the CMC inks, the third mechanism is not likely to contribute to the results under 1/16 FS humidity condition. The increase in roughness for the 1/16 and 1/8 FS levels points out to the emergence of another mechanism at these highly saturated levels. This result can be attributed to aerosolized water droplets falling on the deposited ink filaments and generating low concentration regions on the surface as illustrated in Fig. 3(b). Marangoni flow instabilities are then possible in these regions due to reduced ink viscosity, leading to the observed surface roughening.

To gain a better insight into these different mechanisms, lines were printed at ambient and 1/16FS conditions at 1, 2 and 3 mm/s printing speeds. The surface roughnesses of these lines is presented in Fig. 9(b) which shows that the speed influences the surface roughnesses differently for the ambient and oversaturated conditions. For ambient humidity, the roughness increases with decreasing speed. Explanation for this result could be as follows: At constant flow rate, the total volume of deposited material increases with decreasing speed. Even though the ink drying rate would not change with higher ink volume, the total time to

dry would accordingly increase at lower speeds. This leads to larger number of disturbances on the aforementioned skin formed on the ink surface due to bursting of the trapped solvent. For the 1/16FS case, the roughness decreases with decreasing printing speed. This can be attributed to larger amount of aerosolized water drops being deposited on to the ink surface per unit length and associated smoothening of the concentration gradient at the surface observed at higher speeds.

3.3. DIW pillar print experiments

Fig. 10 shows the SEM images of the rectangular prism-shaped pillars fabricated at varying humidity conditions and constant printing speed and dispensing pressure. Ambient humidity and temperature measured during each of these printing experiments is listed in Table S3. It should be noted that accurate fabrication of these pillars out of a solvent-based ink requires optimization of various parameters including flow rate, printing speed and the dwell time between the layers during which the solvent evaporates. This optimization task is beyond the scope of this paper, however, under constant pressure and printing speed, effect of the humidity condition on the layer-by-layer formation of a 3D object can be qualitatively observed. The pillars fabricated at the ambient conditions exhibit a high level of porosity, which is reduced by the introduction of aerosolized water. At undersaturated conditions, a distinct "crater" can be observed at the center of the pillars which is progressively reduced with increasing flow rate of aerosolized water at oversaturated conditions. Finally, the aerosolized water led to increased spreading of the lower layers.

The porosity and the crater formation can be attributed to the higher drying rate in low humidity conditions leading to higher rate of solute advection during the drying process. This effect is amplified for this 3D geometry compared to line prints since the solute advection can happen across the linear filaments deposited side by side to form individual layers. This can lead to agglomeration of the solute in certain sites and formation of voids on other sites within each layer, ultimately generating a porous 3D structure. Conversely, during HCDIW, given the significantly larger size of the humidity nozzle than the printing nozzle, the effective area of the aerosolized water is larger than the currently printed filament as illustrated in Fig. 1(b). This effectively reduces the ink drying and solute advection rates across a large area within a given layer. At undersaturated conditions, as the solute advection slows down with increasing humidity, the void formation in individual layers gradually shifts to a more global coffee-ring type effect, leading to the crater formation. While reducing the solute advection related defects in the printed structures, the humidity induced reduction of the drying rate in each layer enables more time for the ink to spread out which causes the broadening of the base of the pillars.

To study the effect of the humidity condition on the layer-to-layer fusion during the printing of these pillars, their sidewall morphology was examined as described in Section 2.6. Fig. 11 shows SEM images of sidewall morphology of pillars printed under ambient (a), 60% RH (b), and 1/32FS (c) humidity conditions. It can be seen that the individual layers can be observed more distinctly at dryer conditions. Fig. 11(d) shows a sample profilometry measurement taken on the sidewalls of the layers printed in ambient and oversaturated conditions. In this profile, each peak, separated by approximately 14 μm, represent every other layer, despite the fact that the layer height used during printing was 7 μm. This is due to the fact that each layer is printed in an alternating direction, thus only even or odd numbered layers are visible on a given face of the pillar. The peak-to-valley heights (PVH) extracted from these profiles under different humidity conditions, averaged over multiple pillars printed in each condition is given in Fig. 11(e). It can be seen that the introduction of the aerosolized water leads to a significant reduction in PVH values, especially in undersaturated conditions (from an average of 300 nm in ambient conditions to ~200 nm in undersaturated conditions), indicating a better layer-to-layer fusion. Interestingly, the PVH value is higher for the oversaturated conditions, with 1/16 FS value being statistically similar to the ambient value. One potential explanation for this result is that the already deposited layers will dilute and further spread as a result of exposure to large amounts of aerosolized water during the printing of subsequent layers. Final positions of the layer boundaries will be subject to variations due to complex pinning effects or layer-to-layer variations of the ink concentration, which will in turn affect the average PVH values.

4. Conclusions and outlook

In this paper, the HCDIW approach is presented, where the micro-environment around the printing nozzle is controlled through

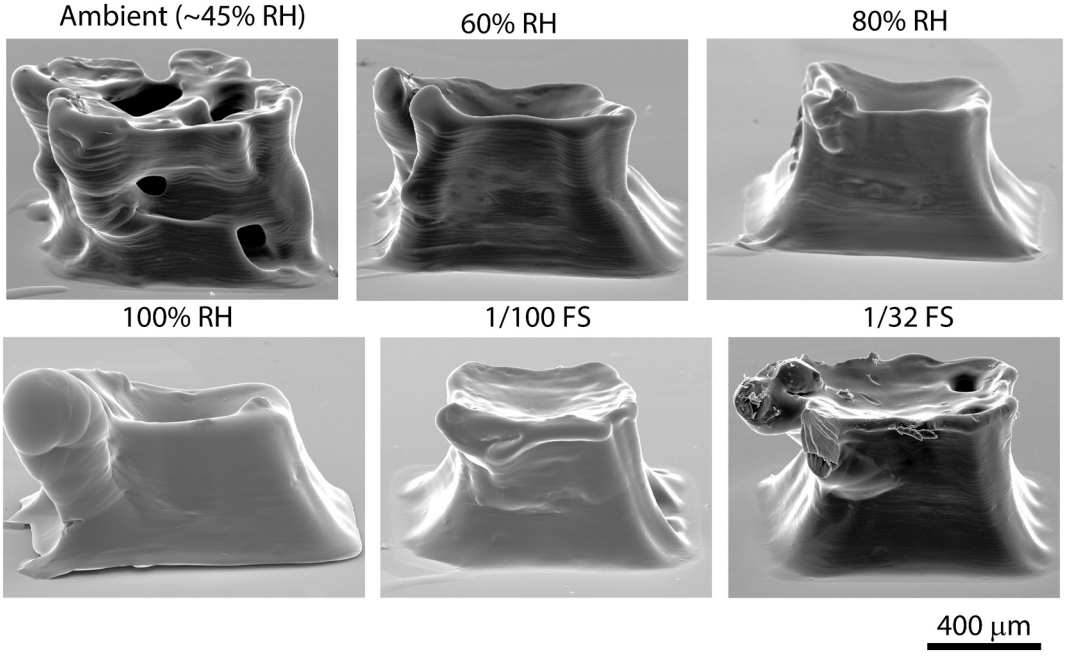

Fig. 10. SEM images of the pillars created under different humidity conditions.

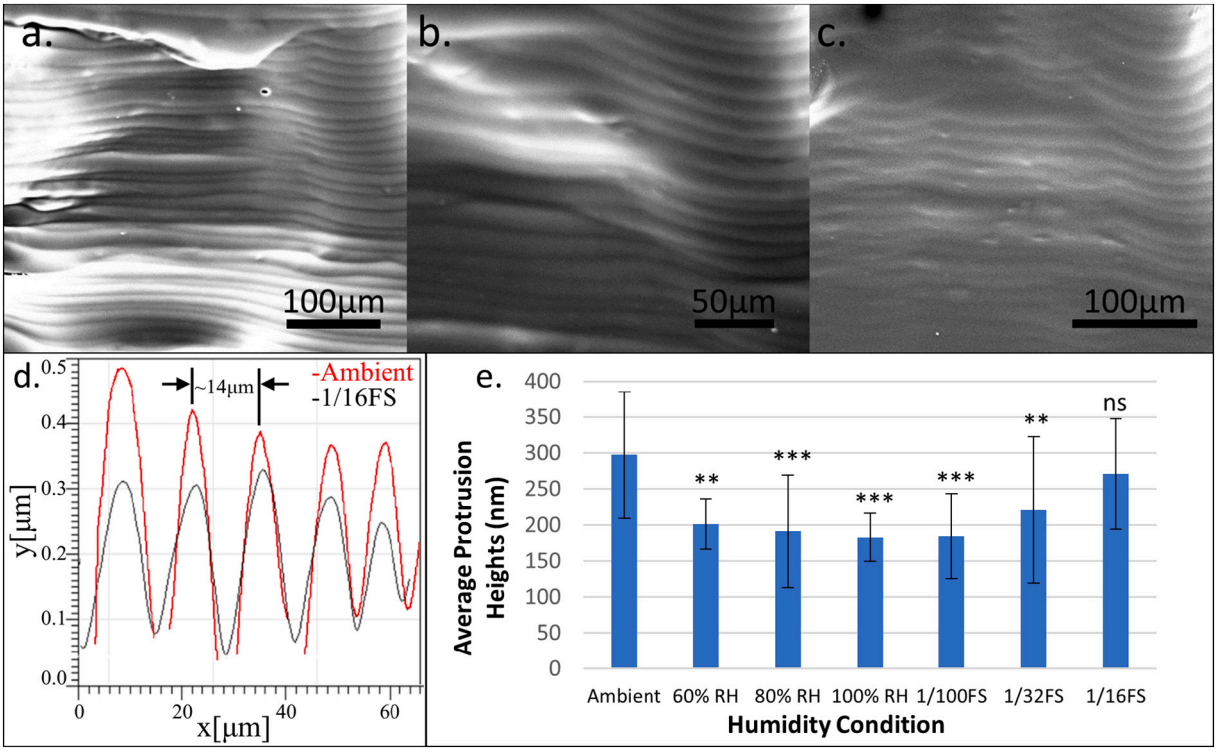

Fig. 11. SEM images of the sidewall morphology of pillars printed at (a) ambient condition, (b) 60% RH, and (c) 1/32FS print pillar, (d) A sample sidewall profilometry measurement, and (e) the peak-to-valley heights (PVH) extracted from these profiles under different humidity conditions.

introduction of aerosolized water to improve the processing of water-based inks, particularly at micro-scales. Our results showed that HCDIW can mitigate the rapid ink-drying related issues such as nozzle clogging, coffee-ring effects, and poor surface quality and layer-to-layer fusion. This is achieved by slowing down the water evaporation during the deposition of the ink filaments either through increasing the relative humidity around the nozzle (undersaturated conditions) or further through depositing aerosolized water droplets on the filaments in oversaturated conditions. Excessive use of aerosolized water and associated decrease in the deposited ink concentration leads to increased spreading of the ink filaments and associated geometric distortions of the printed objects, indicating that the humidity condition needs to be optimized for different printing process parameters, ink compositions and ambient conditions.

These findings show that HCDIW carries a potential to significantly improve the resolution of extrusion-based additive manufacturing using water-dissolved polymer inks and hydrogels by mitigating clogging issues with micro-scale nozzles and realizing fabrication of non-porous solid microstructures with high surface quality. This advancement will greatly widen the material space and enable multi-material capabilities of extrusion-based approaches at microscale. This will provide a significant benefit for critical applications including engineered tissue scaffolds by realizing additive manufacturing methods capable of approaching both the heterogeneity and feature size of native tissues.

The initial insights this paper provides on the HCDIW will be built upon through our future studies. These will include studies looking into smaller printing nozzle sizes (10–100 µm diameter) towards testing the hypothesis that the key effects of HCDIW such as improved layer fusion and surface quality will amplify at smaller scales. Furthermore, the effect of the humidity nozzle size on the 3D printed structure geometry and surface quality remains to be investigated. Beyond this, another area of interest to explore is computational modeling of several aspects of the process including ink spreading and layer fusion under various humidity conditions. Finally, the application space of HCDIW could be extended through hydrogel inks that can be cross-linked. For instance, for ionically cross-linked hydrogels such as sodium alginate, the cross-linking agent can be added to the aerosolized water supply [23] to partially cross-link the printed material during the printing process, providing novel ways to control the printed structure geometry.

Declaration of competing interest

The authors declare that they have no known competing financial interests or personal relationships that could have appeared to influence the work reported in this paper.

Acknowledgements

The authors would like to acknowledge the help of WSU Franceschi Microscopy & Imaging Center in SEM imaging.

Funding statement

This work was financially supported by the National Science Foundation (NSF) grant 1825872 and NSF Graduate Research Fellowship Award 1842493.

Appendix A. Supplementary data

Supplementary data to this article can be found online at https://doi.org/10.1016/j.jmapro.2021.07.059.

References

[1] US Food and Drug Administration. Paving the way for personalized medicine: FDA's role in a new era of medical product development. Silver Spring, MD: US Food and Drug Administration; 2013.
[2] Dababneh AB, Ozbolat IT. Bioprinting technology: a current state-of-the-art review. J Manuf Sci Eng Trans ASME 2014;136.
[3] Arslan-Yildiz A, Assal R El, Chen P, Guven S, Inci F, Demirci U. Towards artificial tissue models: past, present, and future of 3D bioprinting. Biofabrication 2016;8:014103.

[4] Yu C, Jiang J. A perspective on using machine learning in 3D bioprinting. Int J Bioprinting 2020;6:4–11.
[5] Ozbolat IT, Hospodiuk M. Current advances and future perspectives in extrusion-based bioprinting. Biomaterials. 2016;76:321–43.
[6] Richards D, Jia J, Yost M, Markwald R, Mei Y. 3D bioprinting for vascularized tissue fabrication. Ann Biomed Eng 2017;45:132–47.
[7] Bediz B, Korkmaz E, Khilwani R, Donahue C, Erdos G, Falo LD, et al. Dissolvable microneedle arrays for intradermal delivery of biologics: fabrication and application. Pharm Res 2014;31:117–35.
[8] Gao G, Huang Y, Schilling AF, Hubbell K, Cui X. Organ bioprinting: are we there yet? Adv Healthc Mater 2018;7:1–8.
[9] Wedin P, Martinez CJ, Lewis JA, Daicic J, Bergström L. Stress development during drying of calcium carbonate suspensions containing carboxymethylcellulose and latex particles. J Colloid Interface Sci 2004;272:1–9.
[10] Bhattacharjee T, Zehnder S, Rowe K, Jain S, Nixon R, Sawyer G, et al. Writing in the granular gel medium. Sci Adv 2015:1–7.
[11] Lewis Ja. Direct ink writing of 3D functional materials. Adv Funct Mater 2006;16:2193–204.
[12] Ellis J, Mavromatos NE, Nanopoulos DV, Sakharov a S. Direct writing of three-dimensional webs. Nature. 2004;428 (1 p following 386).
[13] Jin Y, Compaan A, Bhattacharjee T, Huang Y. Granular gel support-enabled extrusion of three-dimensional alginate and cellular structures. Biofabrication 2016;8.
[14] Highley CB, Rodell CB, Burdick JA. Direct 3D printing of shear-thinning hydrogels into self-healing hydrogels. Adv Mater 2015;27:5075–9.
[15] Jiang J, Xu X, Stringer J. Support structures for additive manufacturing: a review. J Manuf Mater Process 2018;2:64.
[16] Zhu J, Marchant RE. Design properties of hydrogel tissue-engineering scaffolds. Expert Rev Med Devices 2011;8:607–26.
[17] Korkmaz E, Friedrich EE, Ramadan MH, Erdos G, Mathers AR, Ozdoganlar O Burak, et al. Therapeutic intradermal delivery of tumor necrosis factor-alpha antibodies using tip-loaded dissolvable microneedle arrays. Acta Biomater 2015;24:96–105.
[18] Schlesinger E, Johengen D, Luecke E, Rothrock G, McGowan I, van der Straten A, Desai T. A Tunable, Biodegradable, Thin-film polymer device as a long-acting implant delivering tenofovir alafenamide fumarate for HIV pre-exposure prophylaxis. Pharm Res 2016;33:1649–56.
[19] Laguerre O, Lecoq L, Zoz F, Guyot S, Beney L, Flick D. Influence of the air humidity on the drying of a liquid droplet on a solid plate and on bacterial destruction. J Food Eng 2017;212:76–86.
[20] Mujawar LH, Kuerten JGM, Siregar DP, Amerongen A Van, Norde W. Influence of the relative humidity on the morphology of inkjet printed spots of IgG on a non-porous substrate. RSC Adv 2014;4:19380–8.
[21] Tang HS, Kalyon DM. Estimation of the parameters of Herschel-Bulkley fluid under wall slip using a combination of capillary and squeeze flow viscometers. Rheol Acta 2004;43:80–8.
[22] Strawhecker KE, Kumar SK, Douglas JF, Karim A. The critical role of solvent evaporation on the roughness of spin-cast polymer films [1]. Macromolecules. 2001;34:4669–72.
[23] Ahn S, Lee H, Bonassar LJ, Kim G. Cells (MC3T3-E1)-laden alginate scaffolds fabricated by a modified solid-freeform fabrication process supplemented with an aerosol spraying. Biomacromolecules. 2012;13:2997–3003.